Supplemental Information. Andrianne, Assabban *et al.*

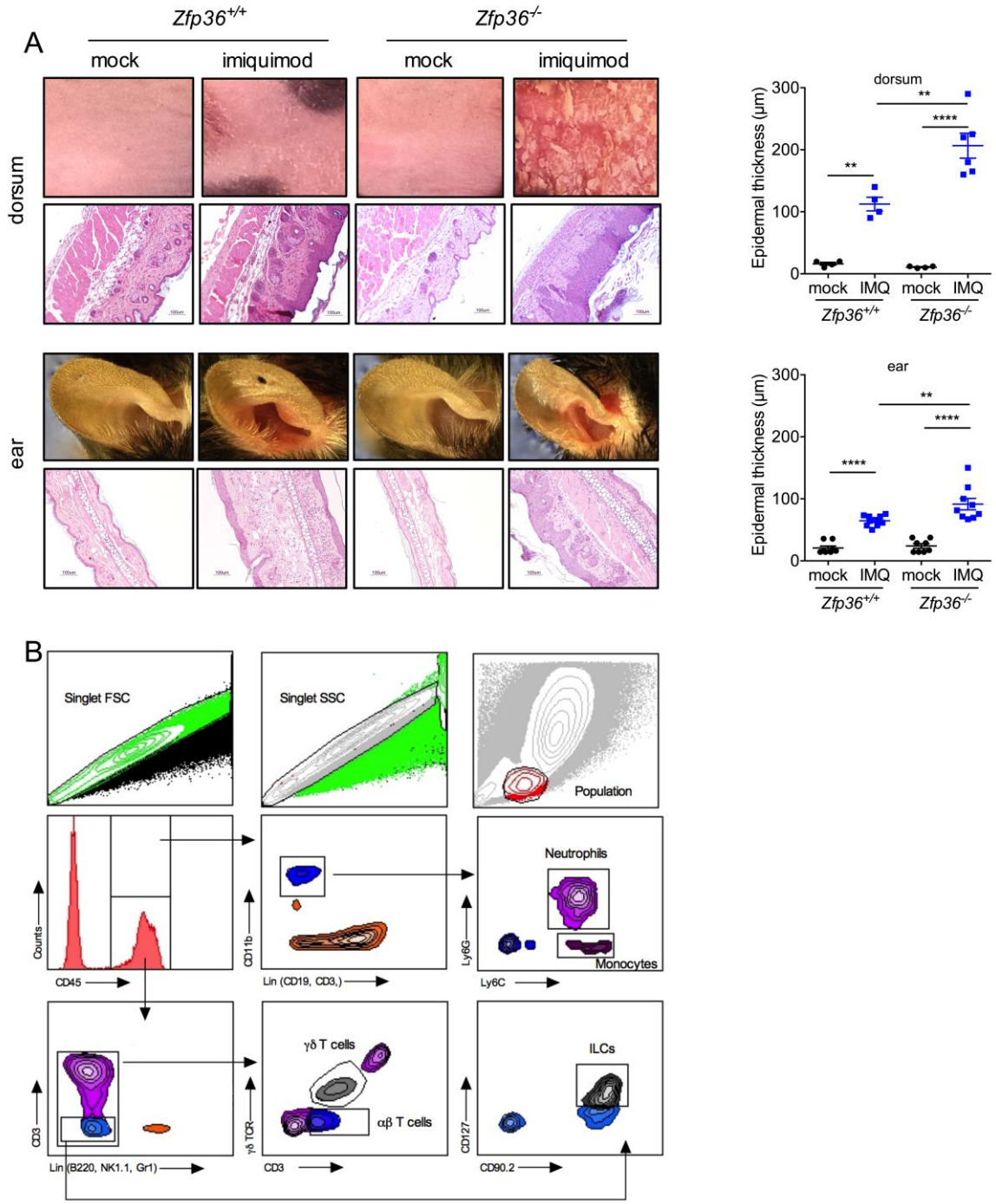

Figure S1. Related to Figure 1. Sensitivity of *Zfp36*$^{-/-}$ mice to Imiquimod treatment following different experimental protocols.
Zfp36-deficient mice (*Zfp36*$^{-/-}$) and their littermates (*Zfp36*$^{+/+}$) were treated topically with Aldara cream during 5 or 7 consecutive days on ears or dorsum, respectively. Skin samples were collected 4h after the last application for analysis of epidermal thickness by histology (A). (B) Gating strategy for skin cells infiltration analysis. Flow cytometry gating strategy is depicted for analysis of neutrophils ($CD45^+$ $CD19^-$ $CD3^-$ $CD11b^+$ $Ly6C^+$ $Ly6G^+$), monocytes ($CD45^+$ $CD19^-$ $CD3^-$ $CD11b^+$ $Ly6C^+$ $Ly6G^-$), αβ T cells ($CD45^+$ $CD19^-$ $NK1.1^-$ $Gr1^-$ $CD3^+$ $\gamma\delta TCR^-$), γδ T cells ($CD45^+$ $CD19^-$ $NK1.1^-$ $Gr1^-$ $CD3^+$ $\gamma\delta TCR^+$) and ILCs ($CD45^+$ $CD19^-$ $NK1.1^-$ $Gr1^-$ $CD3^-$ $CD90^+$ $CD127^+$). Manual gates are depicted as black lines.

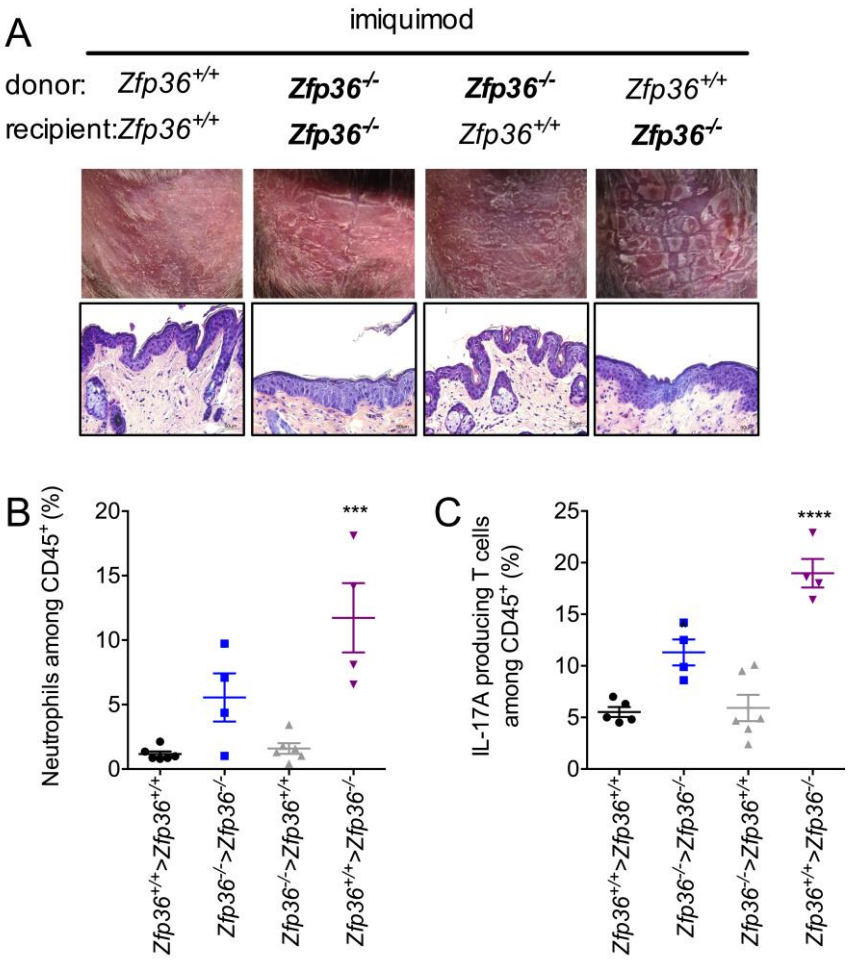

Figure S2. Related to Figure 2. TTP expression in radio-resistant cells is critical for the control of inflammation in imiquimod-induced dermatitis.
Bone marrow chimeric mice (n=6, 5, 6 and 4 mice) were topically treated during 5 consecutive days with imiquimod. Skin samples were collected 4h after the last application for analysis of epidermal thickness by histology (A), cell recruitment by flow cytometry (B), and cytokine production by intracellular protein staining (C). Results are given as mean ± SEM. Statistical significance (**P*<0.05, ***P*<0.01, ****P*<0.001, *****P*<0.0001) was assessed by one-way ANOVA test with Bonferroni correction compared to the *Zfp36*$^{+/+}$>*Zfp36*$^{+/+}$ imiquimod-treated group. Results are representative of 2 experiments.

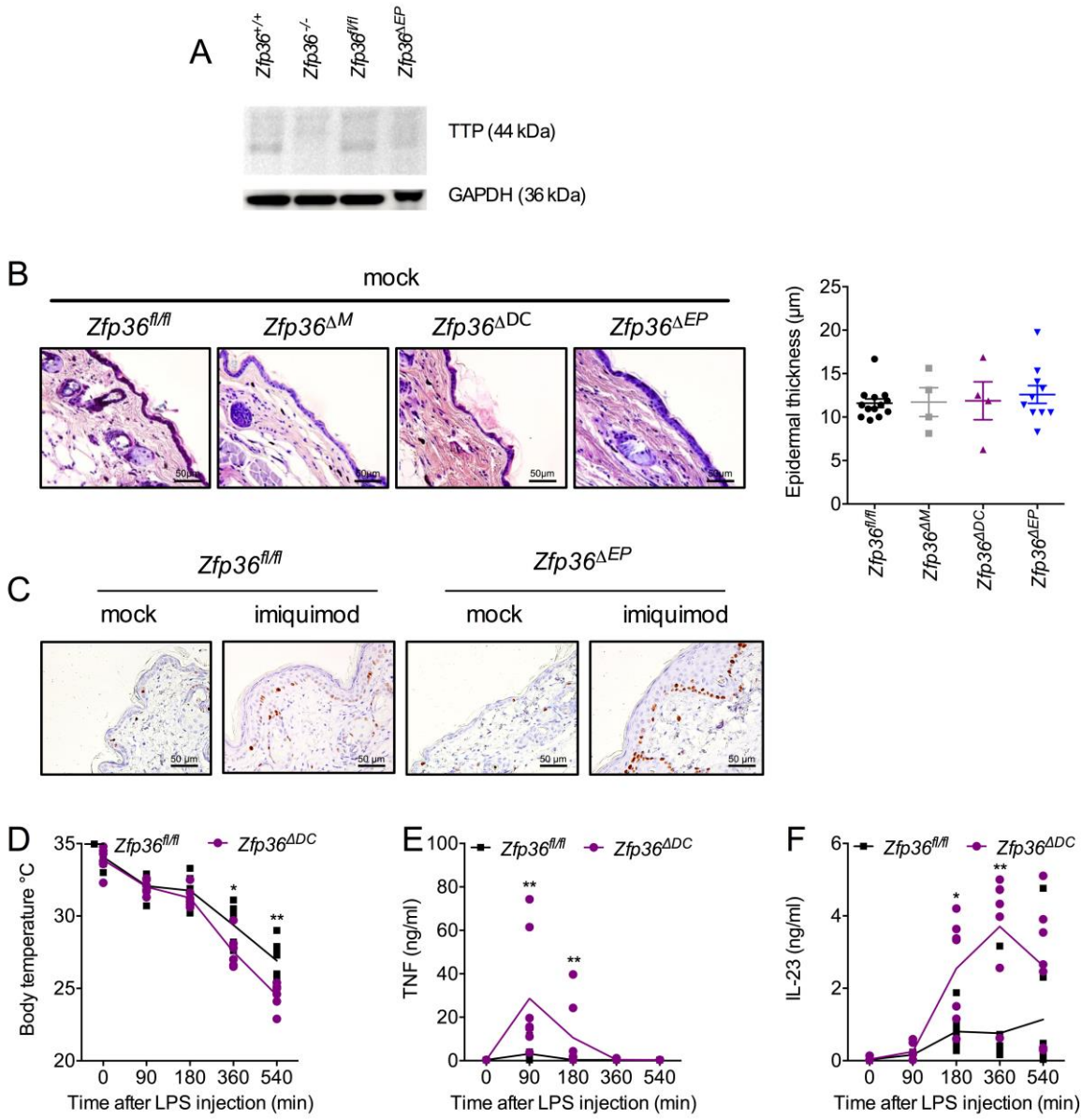

Figure S3. Related to Figure 2. Mock-treated conditions and hypersensitivity of *Zfp36*$^{\Delta DC}$ mice to LPS-induced shock.

TTP level from skin of *Zfp36*$^{+/+}$, *Zfp36*$^{-/-}$, *Zfp36*$^{fl/fl}$ and *Zfp36*$^{\Delta EP}$ were analyzed by western blot. (B) Skin from naïve *Zfp36*$^{\Delta M}$ (n=6), *Zfp36*$^{\Delta DC}$ (n=6), *Zfp36*$^{\Delta EP}$ (n=5) and their littermate control *Zfp36*$^{fl/fl}$ (n=12) mice were collected for analysis of epidermal thickness by histology. (C) *Zfp36*$^{\Delta EP}$ (n=3) and *Zfp36*$^{fl/fl}$ (n=3) mice were topically treated during 5 consecutive days with imiquimod. Skin samples were collected 4h after the last application for analysis of Ki67 marker. (200x magnification). (D-F) *Zfp36*$^{\Delta DC}$ mice (n=7) and their littermate control *Zfp36*$^{fl/fl}$ mice (n=7) were injected intravenously with LPS (0.5 mg/kg). Body temperature and protein levels in serum were analyzed at indicated times. (D), Body temperature (E-F), Protein production in serum. Results are given as mean ± SEM. Statistical significance (**P*<0.05, ***P*<0.01) was assessed by Mann-Whitney test compared to *Zfp36*$^{fl/fl}$ group. Results are representative of 2 experiments.

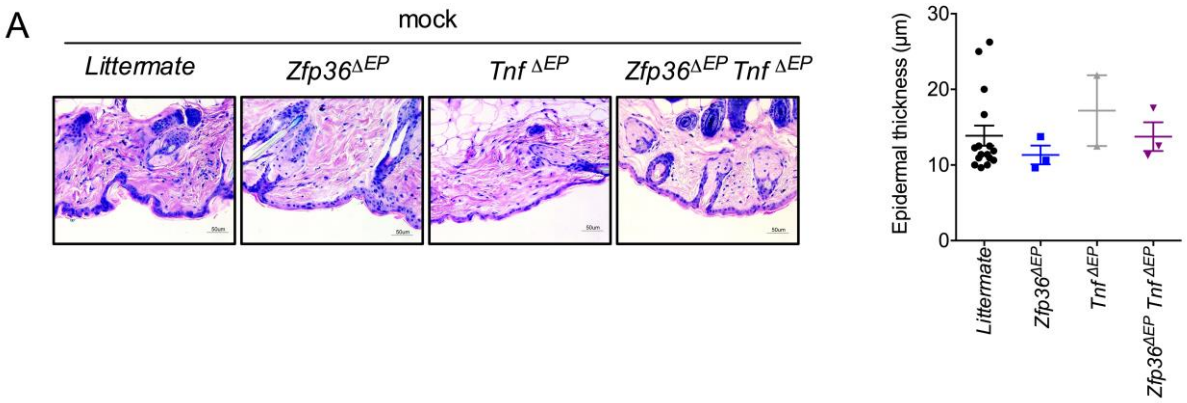

Figure S4. Related to Figure 6. Mock-treated samples.
Skin from *Zfp36*$^{\Delta EP}$ (n=3), *Tnf*$^{\Delta EP}$ (n=3), *Zfp36*$^{\Delta EP}$*Tnf*$^{\Delta EP}$ (n=3) and their littermate control (n=3 for *Zfp36*$^{fl/fl}$, 3 for *Tnf* $^{fl/fl}$ and 3 for *Zfp36*$^{fl/fl}$*Tnf* $^{fl/fl}$) were collected for analysis of epidermal thickness by histology (A). Results are given as mean ± SEM. Statistical significance was assessed by one-way ANOVA test. Results are representative of 2 independent experiments.

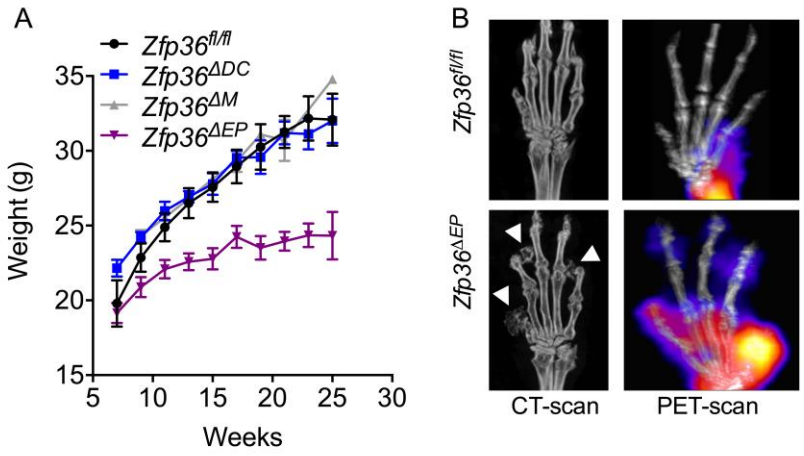

Figure S5. Related to Figure 7. *Zfp36*$^{\Delta EP}$ mice display local bone disruption and hypermetabolism.
(A) Weight curves of *Zfp36*$^{\Delta DC}$ (n=9), *Zfp36*$^{\Delta M}$ (n=5), *Zfp36*$^{\Delta EP}$ (n=13) male mice and their control littermate (*Zfp36*$^{fl/fl}$) (n=22). (B) Representative high resolution CT scan and PET-CT scan of front paws of age- and sex-matched *Zfp36*$^{fl/fl}$ and *Zfp36*$^{\Delta EP}$, injected with [^{18}F]-Sodium Fluoride. Arrows indicate bone disruption.

Supplemental Experimental Procedure

Bone marrow chimera. Recipient mice were irradiated in two runs (6Gy) separated by 4h and reconstituted with bone marrow cells (4×10^6 cells intravenously). Mice were analyzed 3 months after bone marrow transplantation and the degree of chimerism was assessed by measuring CD45.1 and CD45.2 expression by leukocytes using flow cytometry as previously described[50]. The protocol yielded >99% of reconstitution for myeloid population ($CD11b^+$) and >80% of reconstitution for lymphoid cells ($CD3^+$) in the blood.

LPS challenge. Male mice (12-15 weeks) were injected intravenously with LPS at a dose of 0.5 mg/kg (LPS-EB Ultrapure 0111:B4, Invivogen) in 200µl of sterile PBS. Body temperature was measured rectally on anesthetized mice. Blood samples were collected through retro-orbital sinus bleeding of anesthetized mice

Cytokines production. IL-23 and TNF serum levels were determined by ELISA (Duoset, R&D systems).

PET-CT imaging. [^{18}F]-NaF was synthesized at the PET/Biomedical Cyclotron Unit of the Nuclear Medicine Department at ULB-Hôpital Erasme (Bruxelles, Belgium). Mice were injected intravenously (in the lateral tail vein) with 3.9–5.5 MBq of [^{18}F]-NaF. [^{18}F]-NaF PET-CT imaging was performed on a preclinical PET-CT scanner (nano PET/CT with Nucline v1.07 (Build 020), Mediso, Hungary). CT images were obtained for localization, as well as for attenuation and scatter correction of PET images (CT acquisition parameters: maximal field of view, 55 kV, 145 µA, 1100 ms per projection, 180 projections per rotation, 16-to-1 frame binning and pitch of 1 with constant statistics, providing an isotropic reconstructed voxel size of 283 µm). PET images were acquired for 15 minutes, 90 minutes post-injection (3-to-1 coincidence mode with packet time stamps, normal count rate), and reconstructed using a three-dimensional Ordered Subsets Expectation Maximization (3D-OSEM) algorithm (Mediso Ltd., 4 iterations, 6 subsets, intermediate regularization setting, median filtering period defined from iteration counts) with a voxel size of 0.4 mm. All PET images were also corrected for random counts, dead time and decay. Finally, high-resolution CT acquisitions with an isotropic reconstructed voxel size of 21 µm were performed onto the anterior legs of the mice (acquisition parameters were: maximum zoom, 65 kV, 123 µA, 1100 ms per projection, 360 projections per rotation, 4-to-1 frame binning and a pitch of 0.5 with constant statistics; reconstruction with a Ramlak filter and 8 regular samples). The mice were maintained under anesthesia throughout the imaging procedure. VivoQuant 2.5 (InviCRO Ltd, Boston, MA, USA) was used to perform PET-CT analysis.

Table S1: References of the FACS antibodies used in this study

Target	Fluorochrome	clone	isotype	cat Number	Company
B220	APC-eFluor 780	RA3-6B2	Rat IgG2a, k	47-0452-82	eBioscience
CD11b	AF700	M1/70	Rat IgG2b, k	557960	BD Pharmingen
CD127	PE-Cy7	SB/199	Rat IgG2b, k	560733	BD Pharmingen
CD19	APC-Cy7	1D3	Rat IgG2a, k	557655	BD Pharmingen
CD03	APC-Cy7	145-2C11	Hamster IgG1, k	557596	BD Pharmingen
CD3* (complex)	BV421	17A2	Rat IgG2b, k	564008	BD Horizon
CD45	FITC	30-F11	Rat IgG2b, k	11-0451-82	eBioscience
CD90.2	AF700	30-H12	Rat IgG2b, k	105320	Biolegend (ImTec)
gamma delta TCR	PerCP-eFluor710	eBioGL3	Hamster IgG	46-5711	eBioscience
LY6G/LY6C	APC-H7	RB6-8C5	Rat IgG2b, k	557661	BD Pharmingen
IL-17A	AF647	TC11-18H10	Rat IgG1, k	560184	BD Pharmingen
IL-22	PE	1H8PWSR	Rat IgG1, k	12-7221-82	eBioscience
LY-6C	BV421	AL-21	Rat IgM, k	562727	BD Pharmingen
Fc Block (CD16/CD32)	purified	2.4G2	Rat IgG2b, k	553142	BD Pharmingen
NK1.1	APC-Cy7	PK136	Mouse IgG2a, k	560618	BD Pharmingen

Table S2: Sequences of the primers used in this study

	oligo FW 5' to 3'	oligo RV 5' to 3'	Probe 5' to 3'
Cxcl1	F251 : CCG-AAG-TCA-TAG-CCA-CAC-TC (20-mer)	R321 : TTT-CTG-AAC-CAA-GGG-AGC-TT (20-mer)	S275 : AAG-GCA-AGC-CTC-GCG-ACC-AT (20-mer)
Cxcl2	F192 : ACA-TCC-AGA-GCT-TGA-GTG-TGA (21-mer)	R265 : GCC-CTT-GAG-AGT-GGC-TAT-G (19-mer)	S225 : CCC-ACT-GCG-CCC-AGA-CAG-AA (20-mer)
Il1f6	F231 : GTG-TGG-ATC-CTG-CAG-AAC-AA (20-mer)	R315 : GGC-ATG-GGA-GCA-AGG-TAA-TA (20-mer)	S260 : TGC-AGT-CCC-AAG-GAA-AGA-GCA-AAC-A (25-mer)
Il19	F195 : CAG-GAG-CAT-TAA-GCC-TGG-AG (20-mer)	R284 : CTC-TCC-TGA-TGG-TCC-TGG-AA (20-mer)	S220 : TGC-TGC-ATG-ACC-AAC-AAC-CTG-C (22-mer)
Il22	F326 : ACA-GGT-TCC-AGC-CCT-ACA-TG (20mer)	R414 : GTC-GTC-ACC-GCT-GAT-GTG (21mer)	S353 : TGG-TAC-CTT-TCC-TGA-CCA-AAC-TCA-GCA (21mer)
Il23a	F321 : CCC-GTA-TCC-AGT-GTG-AAG-ATG (21-mer)	R448 : CCC-TTT-GAA-GAT-GTC-AGA-GTC-A (22-mer)	S350 : CCA-CAA-GGA-CTC-AAG-GAC-AAC-AGC-C (25-mer)
S100a8	F3 : CCT-TTG-TCA-GCT-CCG-TCT-TC (20-mer)	R82 : CAA-GGC-CTT-CTC-CAG-TTC-AG (20-mer)	S37 : AAG-GAA-ATC-TTT-CGT-GAC-AAT-GCC-G (25-mer)
S100a9	F48 : AGC-CTT-GAG-CAA-GAA-GAT-GG (20-mer)	R129 : TTG-ATG-GAA-GGT-GTC-GAT-GA (20-mer)	S89 : TGG-AGC-GCA-GCA-TAA-CCA-CCA (21-mer)
Il17a	F185 : GCT-CCA-GAA-GGC-CCT-CAG (18-mer)	R324 : CTT-TCC-CTC-CGC-ATT-GAC-A (19-mer)	S206 : ACC-TCA-ACC-GTT-CCA-CGT-CAC-CCT-G (25-mer)
Tnf	F226 : CAG-ACC-CTC-ACA-CTC-AGA-TCA (20mer)	R303 : CAC-TTG-GTG-GTT-TGC-TAC-GA (20mer)	S259 : TCG-AGT-GAC-AAG-CCT-GTA-GCC-CA (23mer)
Zfp36	F343 : CTC-AGA-AAG-CGG-GCG-TTG-T (19-mer)	R419 : GAT-TGG-CTT-GGC-GAA-GTT-CA (20-mer)	S372 : CCA-AGT-GCC-AGT-TTG-CTC-ACG-GC (23-mer)
Cxcl10	F52 : GCC-GTC-ATT-TTC-TGC-CTC-AT (20-mer)	R178 : GCT-TCC-CTA-TGG-CCC-TCA-TT (20-mer)	S105 : TCT-CGC-AAG-GAC-GGT-CCG-CTG (21-mer)
Actin	F1076 : TCC-TGA-GCG-CAA-GTA-CTC-TGT (21-mer)	R1153 : CTG-ATC-CAC-ATC-TGC-TGG-AAG (21-mer)	S1101 : ATC-GGT-GGC-TCC-ATC-CTG-GC (20-mer)
Hprt	F500: GGA-CCT-CTC-GAA-GTG-TTG-GAT (21mer)	R569 : CCA-ACA-ACA-AAC-TTG-TCT-GGA-A (22mer)	S522 : CAG-GCC-AGA-CTT-TGT-TGG-ATT-TGA-A (25mer)
Gapdh	F430 : ATTGTCAGCAATGCATCCTG (20mer)	R512 : CCTTCCACAATGCCAAAGTT (20mer)	S470 : CCCTGGCCAAGGTCATCCATGA (22mer)